On the Extraction of Microseismic Ground Motion from Analog Seismograms for the Validation of Ocean-Climate Models

Thomas Lecocq, Fabrice Ardhuin, Fabienne Collin, Thierry Camelbeeck

On the Extraction of Microseismic Ground Motion from Analogue Seismograms for the Validation of Oceanic-Climatic Models

Lecocq, T.*[1], Ardhuin, F.[2], Collin, F.[1], and Camelbeeck, T.[1]

[1]*Seismology-Gravimetry, Royal Observatory of Belgium, 1180 Brussels, Belgium.*

[2]*Univ. Brest, CNRS, IRD, Ifremer, Laboratoire d'Océanographie Physique et Spatiale (LOPS), IUEM, 29280, Brest, France.*

August 2019

Abstract

We report on a pilot demonstration of the usefulness of analogue seismograms to improve the knowledge about ocean storms before the 1980s by providing additional data for the quantitative validation of ocean wave modelling, in particular for extreme events. We present an automatic digitization method of paper seismograms to extract microseismic ground motion periods and amplitudes. The original paper records are scanned, vectorised and split in minute chunks, as on the original data. The amplitude is calibrated based on the original metadata mentioned on the paper sheets and official bulletins. The digitized time series are processed to extract Power Spectral Densities (PSD) which are compared with modelled seismic noise levels computed using a numerical ocean wave model. As a case study, we focus on 1 month of data recorded at the Royal Observatory of Belgium in January-February 1953, around the "Big Flood", a tragic storm surge that flooded the low lands of England, the Netherlands and Belgium on 1 February 1953. The reconstructed spectrogram for the three components of ground motion (1 vertical and 2 horizontals) evidences clear storm signatures that we relate to specific sources in the North Atlantic ocean. The specific case of the Big Flood evidences a lack of amplitude of the modelled data compared to the observations when the storm reached its maximum in the Southern North Sea. We suggest that the source of seismic noise is related to the primary microseism generated in the North Sea, at periods around 7-8 s. Other discrepancies identified suggest small modifications of the source locations or energy. The coherence between the reconstructed horizontal and vertical ground motions confirms the applicability of the analogue data analysis to the reanalyses of the atmosphere-ocean-solid earth data over the whole 20th century, when only horizontal seismographs were installed at observatories around the world.

*Corresponding author: Thomas.Lecocq@seismology.be

Introduction

Seismologists observed and recorded the Earth's continuous ground motions long before the onset of digital seismography, as early as 1855/1880. Since that time, and until the 1960s to 1980s depending on the observatory, seismic data were recorded analogically, on smoked paper, with ink or on photographic paper. For ocean waves, visual observations from ships make up all the available data until 1946 with a few instrumented records being available, and they only became more common in the 1980s. A global awareness of major ocean storms with wave height measurements only started in 1993 with satellite measurements, but their coverage is not sufficient to catch the peak of storms and our general knowledge of the ocean wave climate heavily relies on numerical models forced by winds from atmospheric reanalyses (Rascle and Ardhuin, 2013; Reguero et al., 2019). Because the wind speed and direction at sea level are diagnostic variables with few measurements before 1994, these estimates and their climatic trends are prone to artificial biases.

Another source of quantitative data comes from the ambient noise recorded by seismometers (Bernard, 1990). Microseism has been extensively studied since the early days of seismology (for a review see Ebeling, 2012, and references therein) mostly because of its ubiquity in all seismic records. Microseism is defined as the continuous ground motions induced by the interaction between the atmosphere, the oceans and the solid Earth (for a complete review see Nakata et al., 2019, and references therein). It has been used to study the regional distribution of its sources, for example by Donn and Blaik (1952) who used a simple tripartite azimuth computation to study the 1950 storm season in the Northern Atlantic, or by Friedrich et al. (1998) using the first digital records of the Gräfenberg Array, Bavaria, Germany (Harjes and Seidl, 1978) to locate multiple sources of microseism in the North Atlantic ocean. The same data was also compiled by Aster et al. (2008, 2010) for studying its long term evolution based on all available digital data from the Seismic Research Observatory, the High-Gain Long Period and Global Seismic Network ((ASL)/USGS, 1972, 1974, 1988).

Using 40 years of seismic records (1954-1998) from Hamburg (Germany), Grevemeyer et al. (2000) showed that changes in the wave climate in the northeast Atlantic Ocean could be inferred from measurements using historical records. Similarly, Dahm et al. (2005) used historical data from different locations in Europe and showed a good correlation between them for specific storm periods. Recently, Gualtieri et al. (2018) showed that tropical cyclones can not only be tracked using the spectral content of the seismic noise, but that their intensity can also be derived from the spectral amplitude. The presence of very long seismic oscillations above 9 s correspond to long ocean wave periods (twice the seismic period, over 18 s) that are the finger prints of extreme ocean storms (Hanafin et al., 2012).

Because the magnitude of microseisms is not simply related to the height of ocean waves (Obrebski et al., 2012, e.g.), it is useful to transform a modeled wave climate into microseism amplitudes. This was done by Stutzmann et al. (2012) to validate a global microseism model. Stopa et al. (2019) used a similar model, transforming wind to waves, and waves to microseisms, for the calibration of a particular atmospheric reanalysis. Here we propose a new seismic digitization method, processing scanned paper seismograms from the analogue instrumental epoch to extract the spectra of the seismic noise. Those spectra, properly referenced in time and

amplitude, are then compared with a microseism model based on the WAVEWATCH III wave model (Tolman and the WAVEWATCH III Development Group, 2014). For this pilot project, we will focus on the "Big Flood" of 1953, a massive storm surge event that dramatically flooded low-lands of the Netherlands, Belgium and England and caused 2165 casualties.

Seismic analogue records

The first seismic records made at the Uccle station of the Royal Observatory of Belgium (ROB) date back to 1898 (Royal Observatory of Belgium, 1985; Van Camp and Camelbeeck, 2004) and were acquired using a von Rebeur-Ehlert triple horizontal pendulum built by Bosch (Strasbourg, France). At the beginning of the XXth century, the ROB owned two Wiechert seismometers: one 1000 kg horizontal (installed in 1910) and one 1300 kg vertical (1911) seismometer, two Galitzin double-pendulum horizontal seismometers (1911-1914 and 1919-1962) and one Galitzin-Wilip vertical seismometer (1930). This vertical seismometer was very difficult to stabilise and essentially useless between 1930 and 1935 (Somville, 1930, and the following years until 1935) until it was heavily modified by Somville in 1936 (Somville, 1936, 1937a,b) to be stable at different periods while insuring that the damping and recording remain identical to the original Galitzin-Wilip.

The Wiechert seismometers used a pen to scratch rolls of smoked paper as recorder, while Galitzin seismometers used a galvanometric system to direct a beam of light toward photographic paper. The advantage of the photo records over smoked paper is the much larger contrast between the trace and the background, which could be greyish or scratched on smoked paper. The friction of the pen on the paper also alters the quality of the records, although this effect is more important for the large amplitudes of seismic events than for background noise records.

The ROB still owns most of the analogue records, either in paper form stored in 1 wooden box per year of data, or digitized on microfilm, which could also be scanned in the future, depending on their preservation state.

Digitizing paper seismograms and extracting ground motion

Extracting digital seismic traces from scans (images) has been the subject of numerous articles in the past 20 years and their digitizing process can be classified in two categories, either manual by clicking all the wiggles of a seismic trace (e.g. Bromirski and Chuang, 2003; Pintore et al., 2005), or automatic using image processing techniques to extract the wiggles (e.g. Baskoutas et al., 2000; Church et al., 2013; Wang et al., 2014). Bromirski and Chuang (2003) show an example on their website (`http://iodlabs.ucsd.edu/peter/seismology/SeisDig.html`, last accessed August 2019) of scanned seismograms from a Wilip-Galitzin vertical seismometer for January 1941 and highlight its similarity with spectrograms that can be obtained nowadays with modern digital seismic data.

Our method is very similar to the one described in Wang et al. (2014) and is composed of the following steps, with new steps developed in this study marked with a *: Scan, Colour inversion, Thresholding*, Binarization,

Rotation*, Region ”labelling”*, Line Thinning - Skeletonization and ObsPy `Trace` object creation*. These steps are described in the following Section. The whole digitization process is written in Python and makes use of state of the art Python modules and available as Jupyter Notebooks (see Data & Resources).

Scanning paper seismograms

The scanning of paper seismogram is a tedious work, but is essential for the conservation of our archives (Okal, 2015). Until recently, ROB scans were restricted to those specific sheets where significant events were recorded. For this study, seismograms were scanned using a Contex HD Ultra scanner capable of ingesting a 841 mm-wide sheet of paper (width of an A0 ISO 216 standard). Such a scanner supports scanning photographic paper, but not smoked paper as these could be damaged by the paper drive rollers. The final image is saved to TIFF file format with convenient naming allowing to store the station name (e.g. UCC), the orientation of the seismometer (’v’, ’n-s’ or ’e-w’) and the date of the record. For processing noise records, a resolution of 300 dpi is sufficient and is less computationally expensive during the processing than 1200 dpi, i.e. the maximal resolution of the scanner.

Colour inversion, thresholding, binarization and rotation

Smoked paper seismograms have a black background (the smoke) and whitish traces, scratched by the pen, while developed photographic papers have a white background and a black trace. In order to easily identify the traces using the same algorithm, the photographic images are inverted to obtain white traces. A threshold (Otsu, 1979) is applied to the image in order to reject small under-represented tones from the image. The image is finally binarized, i.e. all positive values (traces) are set to 1 and the background to 0.

To ease the trace sorting, we rotate the image to account for slight misalignment of the sheet in the scanner. This step is done using a Hough Transform (Hough, 1962; Duda and Hart, 1972), i.e. a computer vision technique to automatically identify straight lines in an image. We only compute the transform for angles in a ± 5 $^\circ$ range. The technique outputs identified lines, described by their location and angle. The image is then rotated by the median angle to horizontalise the traces.

Region labelling and skeletonization

The time encoding on paper seismogram is generally done by one of the three following ways: (1) a gap of 1 or more seconds at the end of each minute, generated by lifting the needle off the smoked paper or by intercepting the light beam to photographic paper; (2) a spike or (3) a translation of a few millimetres of the trace. Our Galitzin records are of type 1: the photographic records show 1 second gaps at the end of every minute.

The ”labelling” operation consists of identifying regions of the image that are connected and form a shape, in our case, continuous chunks of seismic traces. The regions have coordinates in the image space and can therefore be located and sliced easily for further processing. This processing will only occur if the region identified is long and narrow, as we expect short and wide regions to contain bad data, glitches, handwriting or else.

A process of line thinning is then required in order to reduce a two-dimensional region of an image containing an object of random shape to a simple line. 2D objects can be defined by their ”skeleton”, or ”central line”. In the case of seismic records, this skeleton will be centred in the white pixels of the trace. Once identified, each trace is stored together with its (x,y) coordinates on the image.

ObsPy Trace creation

The identified seismic traces are analysed using standard modern processing, which is be done by creating one ObsPy Trace object per trace. The x and y location of the traces are used to sort them time wise and the length of each trace is 59 seconds. To evaluate the sampling rate of each trace, we consider the median length of all traces identified on one sheet and compute the number of pixels per second (pps), which is the sampling rate. All traces are then linearly detrended, resampled (interpolated) to 8 Hz using a Lanczos interpolation, tapered with a 0.5 s taper on both ends and highpass-filtered above 0.08 Hz (12.5 s). The start time of each trace is computed from its (x,y) location.

Instrument response correction

The functioning and the instrument response of the Galitzin seismometers are known and documented in the official Bulletins of the ROB (Somville, 1922a,b). Table 1 shows the parameters for the Galitzin seismometers as in 1953.

Using Table 1 and Galitzin's formulations (Galitzin, 1911, pp 107-108), we can recompute the real ground motion (x_m) from the measured amplitudes on the paper (y_m), i.e. amplitude instrumental response for different periods (T_p):

$$x_m = C_1(1+u_1^2)(1+u^2)\sqrt{1-\mu^2 f(u)}\frac{y_m}{T_p} \quad (1)$$

with $C_1 = \frac{\pi l}{kA_1}$, $f(u) = \left[\frac{2u}{1+u^2}\right]^2$, and $u = \frac{T_p}{T}$, $u_1 = \frac{T_p}{T_1}$

The amplitude response of the Galitzin seismometers (Figure 1) allow for studying the microseism because they have a maximal sensitivity in the primary (secondary) microseism band for the horizontal (vertical) Galitzin, respectively.

Since the very beginning of their usage, the Galitzin seismometers were subject to critics about the non-validity of the assumption that the recorded data was exactly the ground displacement because the coils and the galvanometer had the same eigenperiod (McComb and Wenner, 1936; Wenner and McComb, 1936). There is indeed a difference in phase between the two when the period of the recorded waves are larger or smaller than the nominal frequency. This was also verified by Somville for the Galitzin-Willip vertical seismometer owned by the ROB. The phase shifts observed are orders of magnitude smaller than the studied period (0.1 s shift or less at 1.0 s). This could have a strong impact on phase arrival time measurements, but is negligible for the study of the average microseism periods and amplitudes of minutes to hours.

The dominant period of each 1-minute trace is extracted from its PSD (see below) and is used in Equation 1 to obtain the amplification factor, i.e. removing the instrument's amplitude response. The Galitzine seismometers and the digitizing technique have very little sensitivity to frequencies above 1 Hz.

Power Spectral Density

The PSD of each seismic trace is computed using Welch's method (Welch, 1967). This methods is known to reduce noise in the power spectra at the expense of reducing the frequency resolution because of frequency binning, which is efficient for obtaining information on the broad second microseismic peak.

The Welch method proceeds by splitting the signal in overlapping segments that are then windowed, in our case with a Hanning Window (Blackman and Tukey, 1958), which enhances the importance of the data at the centre of the window. The windowed segments are then converted to a periodogram using the squared magnitude of the discrete Fourier Transform. Individual periodograms are then averaged to reduce the variance of the power measurements.

The final product of our processing are three-hour medians of the individual PSDs. This granularity was chosen to match the one provided by the ocean modelling.

Ocean microseism generation modelling

Our microseism model is a combination of a numerical wave model and a transformation of wave spectra into microseisms. The wave model is described in Rascle and Ardhuin (2013) and covers the world ocean, with a spatial resolution of 0.5 degree in longitude and latitude. The choice of parameterizations for the wind-wave generation and dissipation is particularly important for the directional distribution of the wave energy and the resulting amplitude of microseism sources (Ardhuin et al., 2011). It is forced by winds from the ECMWF 20 century reanalysis (Poli et al., 2016). Based on satellite-derived wave heights for the year 2001, the wind-wave coupling coefficient $\beta_{\max}$ was set to 1.7, giving a good representation of even the extreme wave heights (Stopa et al., 2019). The wave model was run with and without shoreline reflection coefficient R for the wave energy.

The transformation of wave spectra to microseisms follows Ardhuin et al. (2011), with a summation of microseism sources along great circle paths and an attenuation with a constant Q coefficient. For the ROB location in Uccle, Belgium, we have used $Q = 200$ or $Q = 300$ and $R = 0.1$. For the year 2001 to 2014, these constant coefficients typically give a correlation coefficient $r = 0.95$ between the measured vertical ground displacement standard deviation over 3 hours and the modeled value of the same parameter, meaning that the modeled events correspond to the ones observed a the ROB. This processing predicts ground motions in a period/frequency band comparable to the one from the Galitzin seismometers. Looking at the spatial distribution of the modeled sources, we thus expect the UCC station to be sensitive to storms in the deep waters off the British isles, the Norwegian coast, south of Iceland along the mid-Atlantic ridge and the northern-western part of the Mediterranean sea.

Microseismic activity in January-February 1953

In the end of January 1953, a storm formed in the North Atlantic ocean (Figure 2) and moved towards the northern tip of Scotland before changing direction to the south-east, in the North Sea towards the southern part of Denmark (Wemelsfelder, 1953; Wolf and Flather, 2005). While moving south-east in the North Sea, and although its low-pressure centre was not exceptionally deep, this storm generated strong winds and, combined with high spring tides, higher-than-usual sustained surge. During the night from 31 January to 1 February 1953, the surge height was maximal in the low-lands of England, The Netherlands and Belgium. Extreme flooding due to dike failures led to a disastrous number of casualties: 1836 in the Netherlands, 307 in the United Kingdom and 22 in Belgium (Gerritsen, 2005). This disaster, called "The Big Flood", was at the origin of the Delta Plan that today protects the Dutch low-lands from future surges (Wemelsfelder, 1953). In Belgium, between 1953 and 1977, more than 3.7 billion Belgian Francs (40 BEF = 1 EUR) were invested to repair and secure dikes and rivers within the Sigma Plan (Ministère des Travaux Publics, 1977). For this case study, we therefore decided to scan the records of the three components of the Galitzin seismometer between 15 January and 15 February 1953, centered on the "The Big Flood".

Despite a few sheets being incomplete or missing (sadly the one containing the 1 February when the storm surge was maximal) the ground motion induced by this storm can still be extracted and PSDs reconstructed. One explanation for the absence of the records during the maximum of the storm this is that the developed paper was unusable due to bad records. This hypothesis is supported by the records done on the horizontal components, which exhibit an extreme amplification of the wiggles on the mornings of 31 January and 2 February. 90 analogue seismograms (1 month, 3 components) were systematically processed using our work flow and provided hourly Power Spectral Densities of the ground motion recorded in Uccle. Figure 3 shows the time evolution of the Power Spectral Density - or spectrogram - of the noise records and of the model generated for the same period. There are five periods of significant microseismic activity higher than the background level at 0.25 μm: 17-21 January, 26-30 January, 31 January - 2 February, 4-5 February and finally 8-12 February.

Discussion

The microseismic activity recorded by the Galitzin and Galitzin-Willip-Somville seismometers in Uccle evidences strong changes during January-February 1953 (Figure 3). The spectrograms are very coherent, which is expected as the amplitude of the ground motions from Rayleigh and Love waves should have a ratio of horizontal to vertical H/V$\approx$1.0 (Darbyshire, 1954; Juretzek and Hadziioannou, 2016). We can therefore average the three spectrograms and take advantage of their slightly different time coverage/gaps. To compare the spectrogram with the modelled ground motion, we extract time series of the total amplitude of the ground motion (displacement, δ_{RMS}) and of the dominant period of the seismic waves from the observed and the modelled data (Figure 5). Spectra (Figure 3) are processed as in Ardhuin et al. (2011), the δ_{RMS} of the noise is defined as the square root of the integral of the noise spectrum:

$\delta_{RMS} = \sqrt{\int_{0.08Hz}^{0.32Hz} F_\delta df_s}$

with F_δ being the power spectrum of the ground displacement and f_s the period of the seismic wave.

There is a good agreement between the ground motion amplitudes and dominant periods, except for the 17-21 January and the Big Flood event (24 January - 2 February). Because of the original granularity of our data set, we also make use of the individual maximum ground motion per minute and analyse its aggregation using the mean, percentile 95 and standard deviations (Figure 5). In the following, we discuss the different events of interest with respect to the modelled noise sources (Figure 4).

The 17-21 January event (E1 on Figures 3, 4 and 5) is missed by the modelling. The model (Figure 4) locates sources close to the Azores, distributed sources between the Azores and the southern tip of Greenland and, at the same time, strong localized sources on the Norwegian coast and around the Shetland Islands. This period corresponds to very strong sources located at the southern tip of Greenland. To obtain larger amplitudes of the modelled ground motion, we should either diminish the attenuation (higher Q) or increase the energy of the source. Changes of Q are not sufficient to significantly increase the effect of this storm, so we suggest that the two broad sources should have been more energetic that currently modelled.

For the 24-25 January event visible on the modelled data, there is a slight increase in the amplitude but the maximum is missed and could not be investigated due to a gap in the data.

The 26-30 January period (E2) corresponds to sources illuminating the whole West coast of Europe, including South Iceland, UK and Ireland together with a broad source in the Norwegian Sea (Figure 4). The model predicts ground motion amplitudes a little lower with less variations than the observed data. The strongest peak in the observed data corresponds to the moments when the modelled seismic sources hit the west coast of UK and Ireland.

The Big Flood, the 31 January - 2 February storm (E3) shows the largest discrepancy between the model and observations. This period corresponds to the motion of the storm around the Northern tip of Scotland and its way down towards the Channel. The highest peak in amplitude and longest seismic waves period are completely missed by the modelling. The difference is almost twofold (1 μm) in amplitude and 1 s in period. The Southern North Sea is characterized by shallow waters (10 to 150 m) where the coupling between ocean waves and the ground is weak and therefore should generate relatively few microseism, which is what the models indeed predicts. The data, however, proves that strong microseismic energy was recorded at the time of the storm. As possible explanations, we tried to increase the Q factor from 300 to 400 for the area because we know from other seismic studies (Camelbeeck, 1985; El Bouch et al., 2002; Van Noten et al., 2017; Mayor et al., 2018) that the attenuation in NE Belgium is very low due to the presence of the WNW-ESE extending Brabant-London massif, but the changes are to subtle to account for the 2x amplitude difference. Another explanation could be that the modelled data concerns secondary microseism, while there were recent evidences that short period (5 - 8 s) primary microseism could be generated in the North Sea (Becker et al., 2019). This would explain the strong energy measured, as well as the dominant period around 7-8 s, coherent with the work of Choi et al. (2018) who calculated the dominant sea wave periods to be between 7 and 9 s during the maximum of the storm. The study

of the primary microseism generation and specifically in the North Sea has started recently (Juretzek and Hadzioannou, 2017; Becker et al., 2019) and should soon provide new modelling theories to compare with our results. The local wind field around the UCC seismic station, also known to generate local sources of seismic noise by its interaction with trees for example, can be ruled out, as most of the seismic energy radiated is done at the first mode of resonance of trees, around a 1 to 5 s maximum (Roux et al., 2018), while higher modes occur at much higher frequency.

The 4-5 February period (E4) corresponds to sources located in the centre of the North Atlantic. The modelled data is slightly higher than the observations but the trends are parallel. To match those, either Q should be lower (more attenuation) or the source should be further away or weaker.

The 8-12 February period (E5) corresponds to the sources located south of Iceland, moving south towards the West coasts of UK and Ireland, then Brittany, Bay of Biscay, Galicia (Spain) and the whole West coast of Spain and Portugal, ending with sources located on the west coast of Sardinia. The model has a +1 day delay on the maximum of the 8-12 February storm. The maximum observed occurred on 10 February, when the storm hit Scotland simultaneously with Galicia and the Bay of Biscay. There could also be parts of the Southern North Sea affected by stronger waves, and the explanation of the lacking primary microseism above could also apply here.

Conclusions

The digitization of analogue seismograms allows reconstructing the evolution of the microseismic energy recorded at one location. Because of its importance for locating earthquakes, the timing of the seismic records is very accurate, which leads to a high granularity of observations. For each minute of digitized data, we are able to produce one Power Spectra Density spectrum. Averaging them by hour or 3 hours, we can compare the seismic energy observations with modelled microseism obtained from the reanalysis of climate data, as done with WAVEWATCH III. Observations from a single seismometer correspond to the sum of pressure sources originating from a radius of a few thousand kilometres around the station, summing up along great circle paths and attenuating with distance. The observations have therefore a very high temporal resolution while integrating spatially.

The analogue seismic data digitized for a 1-month period centered on the tragic Big Flood event that surged in the Low-Lands of the Netherlands, United Kingdom and Belgium exhibits changes in ground displacement amplitude and period. Those features can be directly linked to specific sources in the North Atlantic Ocean, the Norwegian Sea or the North Sea. While the general trends of amplitude and period match, discrepancies have been identified and raise questions. For the Big Flood itself, the failure of the model to accurately reproduce the seismic energy recorded could be explained by a strong local source of primary microseism, not modelled here, with wave periods around 7-8 s. This effect could also explain the 1-day difference in the maximum of the energy observed for the 8-12 February storm. This calls for more research on the topic in order to provide a combined model for primary and secondary microseism. The 4-5 February event also exhibits differences between observed and modelled data and such events are particularly interesting as they are the most difficult to accurately model

due to their remoteness from the shores and thus from most environmental observations.

We show that the amplitude and dominant period of the ground motion displacement can be reconstructed independently using vertical or horizontal seismometers. This will allow going back in time until the very beginning of seismological observations, as horizontal seismographs were the first type of instruments installed worldwide. Analogue seismic data from different observatories can therefore be used to add constraints on atmosphere-ocean-solid Earth couplings, to study different areas of the oceans and to better locate the microseismic sources, just like the recent digital seismic data. Merging analogue and digital data would allow reanalyses over the complete 20th century.

Data & Resources

Analogue seismograms used in this article are the property of the Royal Observatory of Belgium and can be consulted at any time upon request to the ROB.

Scanned analogue seismograms were processed using NumPy (Oliphant, 2006), SciPy (Jones et al., 2001), Scikit-Image (van der Walt et al., 2014), ObsPy (Beyreuther et al., 2010; Krischer et al., 2015) and Pandas (McKinney, 2012). Figures created with MatPlotLib (Hunter, 2007) and maps were plotted using Cartopy (Met Office, 2010). The modelled data from WAVEWATCH III are available from the FTP server of Ifremer: ftp://ftp.ifremer.fr/ifremer/ww3/HINDCAST/SISMO (last accessed August 2019). It comes in NetCDF format (Rew and Davis, 1990) which are read using the NetCDF4-python module (Whitaker et al., 2019). The whole processing has been implemented in Jupyter Notebooks (Kluyver et al., 2016) and is accessible open and free on the authors' GitHub account (https://github.com/ThomasLecocq, last accessed August 2019)

Acknowledgments

C. Hadziioannou is acknowledged for the discussions about the primary microseism in the North Sea. C. Caudron, A. Watlet and K. Van Noten are acknowledged for the discussions and proofreading of the manuscript

The following persons are... ...

References

Ardhuin, F., Stutzmann, E., Schimmel, M., and Mangeney, A. (2011). Ocean wave sources of seismic noise. *Journal of Geophysical Research: Oceans*, 116(C9):C09004.

(ASL)/USGS, A. S. L. (1972). High-Gain Long-Period Network.

(ASL)/USGS, A. S. L. (1974). Seismic Research Observatory.

(ASL)/USGS, A. S. L. (1988). Global Seismograph Network (GSN - IRIS/USGS).

Aster, R. C., McNamara, D. E., and Bromirski, P. D. (2008). Multidecadal climate-induced variability in microseisms. *Seismological Research Letters*, 79(2):194–202.

Aster, R. C., McNamara, D. E., and Bromirski, P. D. (2010). Global trends in extremal microseism intensity. *Geophysical Research Letters*, 37(14).

Baskoutas, I. G., Kalogeras, I. S., Kourouzidis, M., and Panopoulou, G. (2000). A Modern Technique for the Retrieval and Processing of Historical Seismograms in Greece. *Natural Hazards*, 21:55–64.

Becker, D., Kruse, T., Dethof, F., Weidle, C., and Hadziioannou, C. (2019). Microseism in the North Sea: Tidal forcing, H/V-variability and a future monitoring network. *EGU General Assembly, Vienna, Austria*, page 1.

Bernard, P. (1990). Historical sketch of microseisms from past to future. *Physics of the Earth and Planetary Interiors*, 63(3-4):145–150.

Beyreuther, M., Barsch, R., Krischer, L., Megies, T., Behr, Y., and Wassermann, J. (2010). ObsPy: A Python Toolbox for Seismology. *Seismological Research Letters*, 81(3):530–533.

Blackman, R. B. and Tukey, J. W. (1958). The measurement of power spectra from the point of view of communications engineering - Part I. *Bell System Technical Journal*, 37(1):185–282.

Bromirski, P. D. and Chuang, S. (2003). SeisDig: Software to digitize scanned analog seismogram images, user's manual.

Camelbeeck, T. (1985). Some notes concerning the seismicity in Belgium. Magnitude scale. Detection capability of the Belgian seismic stations. In *Seismic activity in western Europe*. P. Melchior, reidel edition.

Choi, B. H., Kim, K. O., Yuk, J.-H., and Lee, H. S. (2018). Simulation of the 1953 storm surge in the North Sea. *Ocean Dynamics*, 68(12):1759–1777.

Church, E. D., Bartlett, A. H., and Jourabchi, M. A. (2013). Raster-to-Vector Image Analysis for Fast Digitization of Historic Seismograms. *Seismological Research Letters*, 84(3):489–494.

Dahm, T., Krüger, F., Essen, H.-H., and Hensch, M. (2005). Historic microseismic data and their relation to the wave-climate in the North Atlantic. *Meteorologische Zeitschrift*, 14(6):771–779.

Darbyshire, J. (1954). Structure of microseismic waves: estimation of direction of approach by comparison of vertical and horizontal components. *Proceedings of the Royal Society of London. Series A, Mathematical and Physical Sciences*, 223(1152):16.

Donn, W. L. and Blaik, M. (1952). A study and evaluation of the tripartite seismic method of locating hurricanes. *Bulletin of the Seismological Society of America*, page 19.

Duda, R. O. and Hart, P. E. (1972). Use of the Hough transformation to detect lines and curves in pictures. *Communications of the ACM*, 15(1):11–15.

Ebeling, C. W. (2012). Inferring Ocean Storm Characteristics from Ambient Seismic Noise. In *Advances in Geophysics*, volume 53, pages 1–33. Elsevier.

El Bouch, A., Camelbeeck, T., and Martin, H. (2002). Atténuation des ondes sismiques en Belgique et dans les régions limitrophes à partir de la coda des tremblements de terre locaux. *Geologica Belgica*, 5(1-2):17–29.

Friedrich, A., Krüger, F., and Klinge, K. (1998). Ocean-generated microseismic noise located with the Gräfenberg array. *Journal of Seismology*, 2(1):47–64.

Galitzin, B. B. (1911). *Ueber ein neues aperiodisches horizontalpendel mit galvanometruscher fernregistrierung*. Buchdr. der K. Akademie der wissenschaften.

Gerritsen, H. (2005). What happened in 1953? The Big Flood in the Netherlands in retrospect. *Philosophical Transactions of the Royal Society of London A: Mathematical, Physical and Engineering Sciences*, 363(1831):1271–1291.

Grevemeyer, I., Herber, R., and Essen, H.-H. (2000). Microseismological evidence for a changing wave climate in the northeast Atlantic Ocean. *Nature*, 408(6810):349–352.

Gualtieri, L., Camargo, S. J., Pascale, S., Pons, F. M. E., and Ekström, G. (2018). The persistent signature of tropical cyclones in ambient seismic noise. *Earth and Planetary Science Letters*, 484:287–294.

Hanafin, J. A., Quilfen, Y., Ardhuin, F., Sienkiewicz, J., Queffeulou, P., Obrebski, M., Chapron, B., Reul, N., Collard, F., Corman, D., and others (2012). Phenomenal sea states and swell from a North Atlantic storm in February 2011: a comprehensive analysis. *Bulletin of the American Meteorological Society*, 93(12):1825–1832.

Harjes, H. and Seidl, D. (1978). Digital recording and analysis of broad-band seismic data at Gräfenberg (GRF) Array. *Journal Of Geophysics-Zeitschrift Fur Geophysik*, 44(5):511–523.

Hough, P. V. C. (1962). Method and means for recognizing complex patterns.

Hunter, J. (2007). Matplotlib: A 2d Graphics Environment. *Computing in Science Engineering*, 9(3):90–95.

Jones, E., Oliphant, T., Peterson, P., et al. (2001). *SciPy: Open source scientific tools for Python*.

Juretzek, C. and Hadziioannou, C. (2016). Where do ocean microseisms come from? A study of Love-to-Rayleigh wave ratios: LOVE-TO-RAYLEIGH RATIOS IN AMBIENT NOISE. *Journal of Geophysical Research: Solid Earth*, 121(9):6741–6756.

Juretzek, C. and Hadziioannou, C. (2017). Linking source region and ocean wave parameters with the observed primary microseismic noise. *Geophysical Journal International*, 211(3):1640–1654.

Kluyver, T., Ragan-Kelley, B., Pérez, F., Granger, B., Bussonnier, M., Frederic, J., Kelley, K., Hamrick, J., Grout, J., Corlay, S., Ivanov, P., Avila, D., Abdalla, S., and Willing, C. (2016). Jupyter Notebooks - A publishing format for reproducible computational workflows. In Loizides, F. and Schmidt, B., editors, *Positioning and Power in Academic Publishing: Players, Agents and Agendas*, pages 87–90. IOS Press.

Krischer, L., Megies, T., Barsch, R., Beyreuther, M., Lecocq, T., Caudron, C., and Wassermann, J. (2015). ObsPy: a bridge for seismology into the scientific Python ecosystem. *Computational Science & Discovery*, 8(1):014003.

Mayor, J., Traversa, P., Calvet, M., and Margerin, L. (2018). Tomography of crustal seismic attenuation in Metropolitan France: implications for seismicity analysis. *Bulletin of Earthquake Engineering*, 16(6):2195–2210.

McComb, H. E. and Wenner, F. (1936). Shaking-table investigations of teleseismic seismometers. *Bulletin of the Seismological Society of America*, 26(4):26.

McKinney, W. (2012). *Python for data analysis: Data wrangling with Pandas, NumPy, and IPython*. " O'Reilly Media, Inc.".

Met Office (2010). *Cartopy: a cartographic python library with a matplotlib interface*. Exeter, Devon.

Ministère des Travaux Publics (1977). Plan Sigma pour la protection du bassin de l'Escaut Maritime contre les marées-tempêtes de la mer du nord. Technical report.

Nakata, N., Gualtieri, L., and Fichtner, A. (2019). *Seismic ambient noise*. Cambridge University Press.

Obrebski, M., Ardhuin, F., Stutzmann, E., and Schimmel, M. (2012). How moderate sea states can generate loud seismic noise in the deep ocean. *Geophysical Research Letters*, 39(11).

Okal, E. A. (2015). Historical seismograms: Preserving an endangered species. *GeoResJ*, 6:53–64.

Oliphant, T. E. (2006). *Guide to NumPy*.

Otsu, N. (1979). A Threshold Selection Method from Gray-Level Histograms. *IEEE Transactions on Systems, Man, and Cybernetics*, 9(1):62–66.

Pintore, S., Quintiliani, M., and Franceschi, D. (2005). Teseo: A vectoriser of historical seismograms. *Computers & Geosciences*, 31(10):1277–1285.

Poli, P., Hersbach, H., Dee, D. P., Berrisford, P., Simmons, A. J., Vitart, F., Laloyaux, P., Tan, D. G., Peubey, C., Thépaut, J.-N., and others (2016). ERA-20c: An atmospheric reanalysis of the twentieth century. *Journal of Climate*, 29(11):4083–4097.

Rascle, N. and Ardhuin, F. (2013). A global wave parameter database for geophysical applications. Part 2: Model validation with improved source term parameterization. *Ocean Modelling*, 70:174–188.

Reguero, B. G., Losada, I. J., and Méndez, F. J. (2019). A recent increase in global wave power as a consequence of oceanic warming. *Nature communications*, 10.

Rew, R. and Davis, G. (1990). NetCDF: an interface for scientific data access. *IEEE computer graphics and applications*, 10(4):76–82.

Roux, P., Bindi, D., Boxberger, T., Colombi, A., Cotton, F., Douste-Bacque, I., Garambois, S., Gueguen, P., Hillers, G., Hollis, D., Lecocq, T., and Pondaven, I. (2018). Toward Seismic Metamaterials: The METAFORET Project. *Seismological Research Letters*, 89(2A):582–593.

Royal Observatory of Belgium (1985). Belgian Seismic Network.

Somville, O. (1922a). Constantes des sismographes galitzine. In *Annales de l'Observatoire Royal de Belgique*, volume 1.

Somville, O. (1922b). Sur la methode d'enregistrement galvanometrique appliquee aux sismographes galitzine. In *Annales de l'Observatoire Royal de Belgique*, volume 1.

Somville, O. (1930). Bulletin Séismique de l'Observatoire royal de Belgique.

Somville, O. (1936). Bulletin Séismique de l'Observatoire royal de Belgique.

Somville, O. (1937a). Bulletin Séismique de l'Observatoire royal de Belgique.

Somville, O. (1937b). Un nouveau type de séismographe vertical. *Publications du Bureau central séismologique international*, Fascicule 15:137–145.

Somville, O. (1953). Bulletin Séismique de l'Observatoire royal de Belgique.

Stopa, J. E., Ardhuin, F., Stutzmann, E., and Lecocq, T. (2019). Sea State Trends and Variability: Consistency Between Models, Altimeters, Buoys, and Seismic Data (1979–2016). *Journal of Geophysical Research: Oceans*, 124(6):3923–3940.

Stutzmann, E., Ardhuin, F., Schimmel, M., Mangeney, A., and Patau, G. (2012). Modelling long-term seismic noise in various environments. *Geophysical Journal International*, 191(2):707–722.

Tolman, H. L. and the WAVEWATCH III Development Group (2014). User Manual and system documentation of WAVEWATCH III version 4.18. Technical Note 316, NOAA/NWS/NCEP/MMAB.

Van Camp, M. and Camelbeeck, T. (2004). Histoire des stations sismiques belges: de la station ≪Solvay≫ au réseau national de surveillance sismique. *Ciel et Terre*, 120(6):162–176.

van der Walt, S., Schönberger, J. L., Nunez-Iglesias, J., Boulogne, F., Warner, J. D., Yager, N., Gouillart, E., and Yu, T. (2014). scikit-image: image processing in Python. *PeerJ*, 2:e453.

Van Noten, K., Lecocq, T., Sira, C., Hinzen, K.-G., and Camelbeeck, T. (2017). Path and site effects deduced from transfrontier internet macroseismic data of two recent M4 earthquakes in NW Europe. *Solid Earth Discussions*, pages 1–33.

Wadey, M. P., Haigh, I. D., Nicholls, R. J., Brown, J. M., Horsburgh, K., Carroll, B., Gallop, S. L., Mason, T., and Bradshaw, E. (2015). A comparison of the 31 January–1 February 1953 and 5–6 December 2013 coastal flood events around the UK. *Frontiers in Marine Science*, 2.

Wang, M., Jiang, Q., and Pan, Z. (2014). A New Curve Tracing Algorithm Based on Local Feature in the Vectorization of Paper Seismograms. *Sensors & Transducers*, 165(2):4.

Welch, P. (1967). The use of fast Fourier transform for the estimation of power spectra: A method based on time averaging over short, modified periodograms. *IEEE Transactions on Audio and Electroacoustics*, 15(2):70–73.

Wemelsfelder, P. J. (1953). The disaster in The Netherlands caused by the storm flood of February 1, 1953. *Coastal Engineering Proceedings*, 1(4):18.

Wenner, F. and McComb, H. E. (1936). The Galitzin seismometer: Discrepancies between the Galitzin theory and the performance of a Wilip-Galitzin seismometer. *Bulletin of the Seismological Society of America*, 26(4):317–322.

Whitaker, J., Khrulev, C., Huard, D., Paulik, C., Hoyer, S., Filipe, Pastewka, L., Mohr, A., Marquardt, C., Couwenberg, B., Whitaker, J., Cuntz, M., Bohnet, M., Brett, M., Hetland, R., Korenčiak, M., barronh, Onu, K., Helmus, J. J., Hamman, J., Barna, A., fredrik 1, Koziol, B., Kluyver, T., May, R., Smrekar, J., Barker, C., da Silva, D., Gohlke, C., and Kinoshita, B. P. (2019). Unidata/netcdf4-python: version 1.5.1.2 release.

Wolf, J. and Flather, R. A. (2005). Modelling waves and surges during the 1953 storm. *Philosophical Transactions of the Royal Society of London A: Mathematical, Physical and Engineering Sciences*, 363(1831):1359–1375.

Authors' full mailing address

- Thomas Lecocq, Fabienne Collin & Thierry Camelbeeck: Royal Observatory of Belgium, Seismology-Gravimetry, Avenue circulaire 3, 1180 Uccle, Belgium
- Fabrice Ardhuin: Univ. Brest, CNRS, IRD, Ifremer, Laboratoire d'Océanographie Physique et Spatiale (LOPS), IUEM, 29280, Brest, France.

Tables

Table 1: 1953 parameters for the Galitzin seismometers at ROB, where T is the period of the pendulum, T_1 the period of the galvanometer, l the reduced pendulum length, μ the damping constant, A_1 the distance of the drum from the galvanometer mirror and k the transfer factor (Galitzin, 1911, p. 103).

Instrument	T (s)	T_1 (s)	l (mm)	μ	A_1 (mm)	k
Galitzin E-W	21.5	21.8	123.8	+0.2	1040	38
Galitzin N-S	24.5	21.8	124.7	+0.2	1040	38
G.-Willip-Somville V	10.0	10.15	173.8	0.0	1060	97

List of Figures

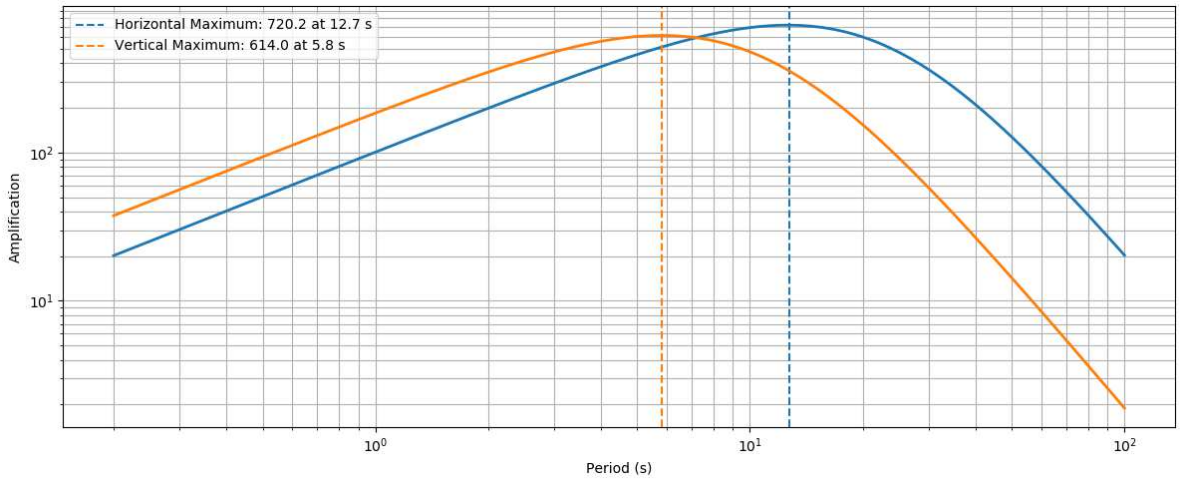

Figure 1: The amplitude response of the Galitzin seismometers owned by the ROB (Somville, 1930, 1937a, 1953)

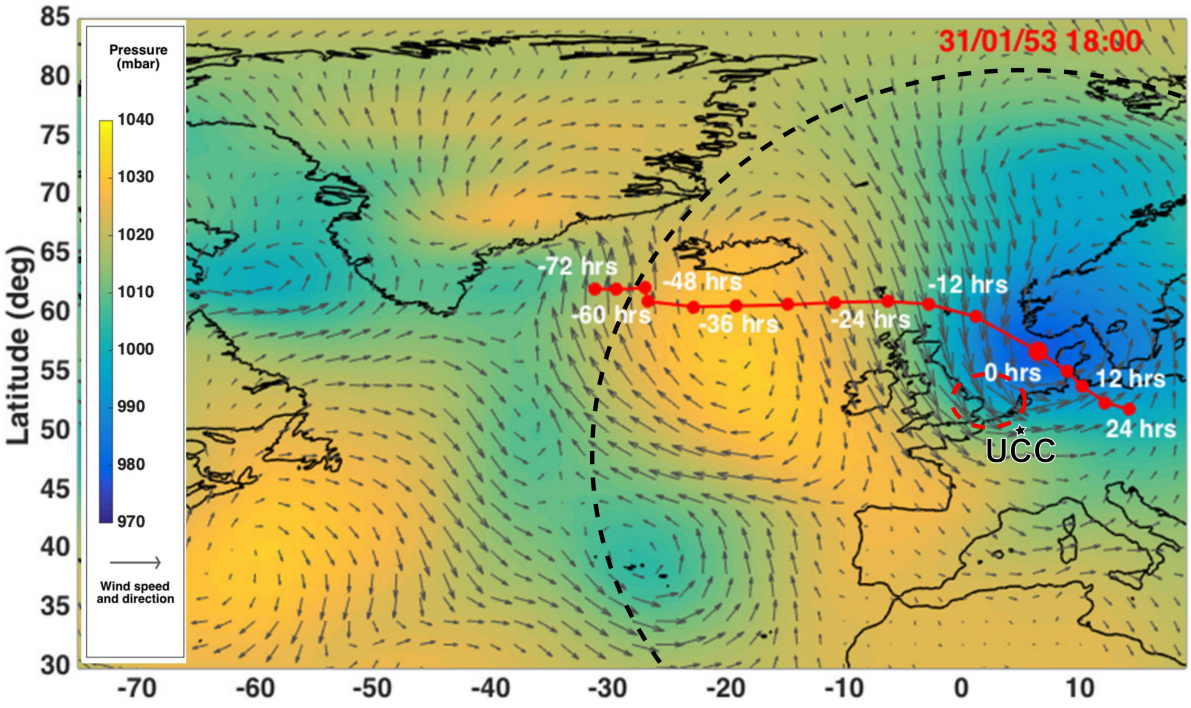

Figure 2: Map of the 1953 storm path 72 hours before until 24 after the Big Flood with the atmospheric pressure and wind fields 6 hours before the Big Flood, redrawn from Wadey et al. (2015). The dashed ellipses indicate the region where dramatic flooding occurred (red) and the area of maximal sensitivity (black) for the UCC seismic station (black star).

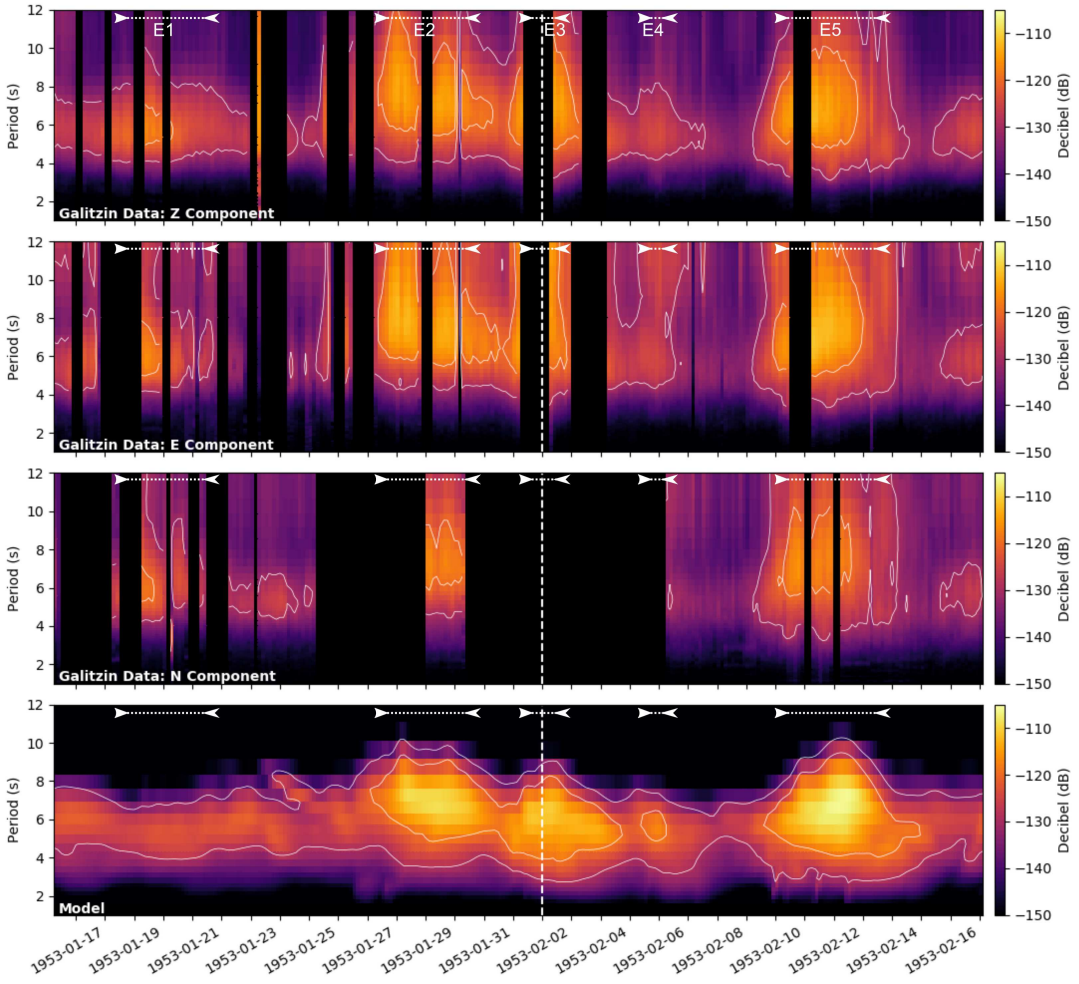

Figure 3: 15 January-15 February 1953 displacement power spectral density (PSD) spectrograms based on the automatically extracted time series for the Vertical, East-West and North-South components, and below, the result of the simulation using WAVEWATCH III and coastal reflections (REF102040). The thin white contours that highlight the -130 and -120 dB levels are indicated for illustration purposes only. The thick dashed white line indicates the time of occurrence of the Big Flood. The arrows indicate the five periods of significant microseismic activity, labelled E1 to E5 in the text and the following figures.

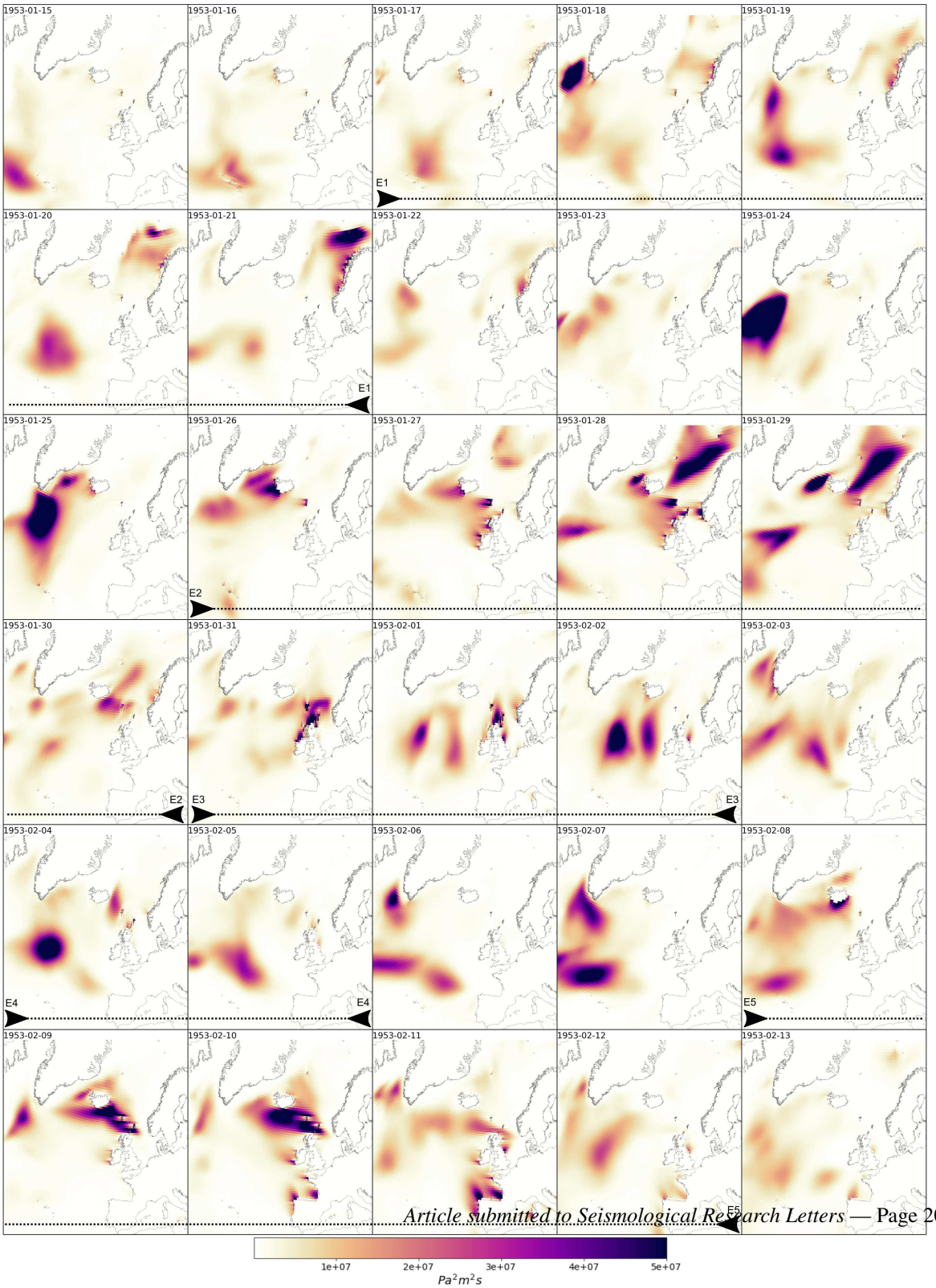

Figure 4: Modelled daily average microseismic sources obtained from Ocean Modelling: the power spectral density of equivalent surface pressure summed over all periods, not corrected for coupling (WAVEWATCH III and coastal reflections REF102040). The arrows indicate the five periods of significant microseismic activity.

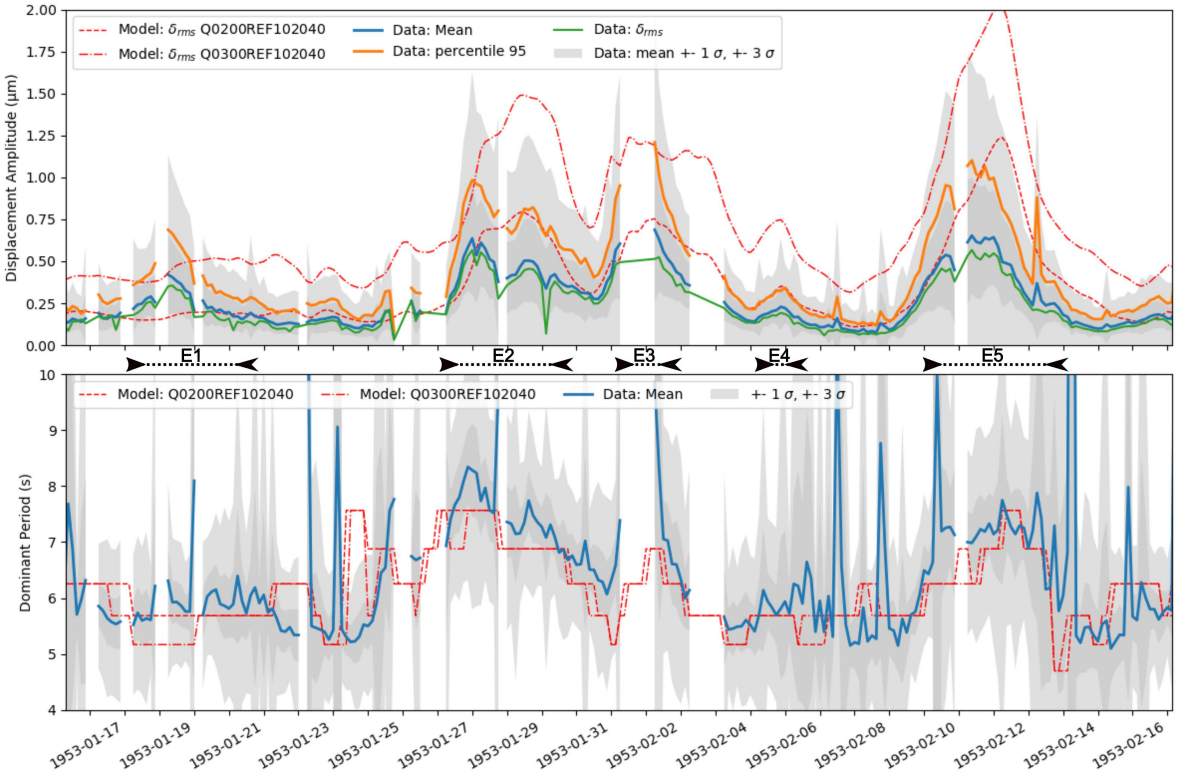

Figure 5: Comparison of the ground displacement amplitude (above) and its dominant period (below) for the modelled and observed data from digitized seismograms of the UCC station. Two ocean generated ground motion models with different Q factor are presented. The arrows indicate the five periods of significant microseismic activity higher than the background level at 0.25 μm: 17-21 January, 26-30 January, 31 January - 2 February, 4-5 February and finally 8-12 February.